

# Systematic characterisation of silicon-embedded accelerometers for mechanomyography

J. Silva<sup>1,2</sup> T. Chau<sup>1,2,3</sup> S. Naumann<sup>1,2,3</sup> W. Heim<sup>3</sup>

<sup>1</sup>Department of Mechanical & Industrial Engineering, University of Toronto, Toronto, Ontario, Canada

<sup>2</sup>Institute of Biomaterials & Biomedical Engineering, University of Toronto, Toronto, Ontario, Canada

<sup>3</sup>Rehabilitation Engineering Department, Bloorview MacMillan Children's Centre, Toronto, Ontario, Canada

**Abstract**—Silicon soft suction sockets (roll-on sleeves) currently used in passive prostheses for below-elbow amputees could also be used in externally powered prostheses, enhancing their functionality and comfort. However, as it is extremely difficult to hold currently used electromyography (EMG) sensors in place reliably within a silicon socket, an alternative measurement of muscular activity as the control input is necessary. Mechanomyography (MMG) is the epidermal measurement of the low-frequency vibrations produced by a contracting muscle. MMG sensors do not have to be in direct contact with the skin. Moreover, the embedding of sensors in the roll-on sleeve may also solve attachment issues, making sensor placement flexible. Therefore the objective was to determine the feasibility of recording MMG signals using silicon-embedded, micro-machined accelerometers. Fifteen embedded accelerometers were excited with predefined vibration patterns. The signal-to-noise ratio (SNR) and frequency response of each sample were measured and compared with those of non-embedded accelerometers. The SNR of embedded samples ( $\cong 19$  dB) was significantly higher than that of non-embedded samples ( $\cong 12$  dB), owing to the considerable mechanical damping effect of the silicon in the 300–900 Hz bandwidth ( $p=0.0028$ ). This has implications for the application of silicon-embedded accelerometers for externally powered prosthesis control.

**Keywords**—Mechanomyography, Soft silicon suction sockets, Prosthesis control

Med. Biol. Eng. Comput., 2003, 41, 290–295

## 1 Introduction

### 1.1 Soft as against rigid sockets

A SCHEMATIC diagram of the constitutive parts of an externally powered below-elbow prosthesis is shown in Fig. 1. The socket is the part of the prosthesis in direct contact with the patient's residual limb. Therefore its shape and size depend on the particular characteristics of the amputee's stump.

Current, externally powered prostheses are dispensed with rigid supercondylar sockets encompassing the elbow condyles to suspend the total weight of the prosthesis. An example is shown in Fig. 2a. EMG sensors are fastened flush in the socket wall and positioned precisely over the muscle bulk. A hard shell, which holds the terminal element and acts as the actual forearm, covers the hard socket.

Advances in socket design have led to the creation of mouldable silicon suction sockets or roll-on silicon sleeves, as shown in Fig. 2b. These silicon sleeves provide significant advantages over rigid supercondylar sockets. Comfort is improved, because the total weight of the prosthesis is distri-

buted along the residual limb instead of resting exclusively over the elbow condyles. Functionality is also enhanced, because roll-on sleeves preserve natural pronation and supination of the forearm in below-elbow amputees. However, silicon sleeves are not currently prescribed with externally powered prostheses, as EMG sensors cannot be reliably held in place over the muscle bulk (GABER *et al.*, 2001). Research into alternative channels for

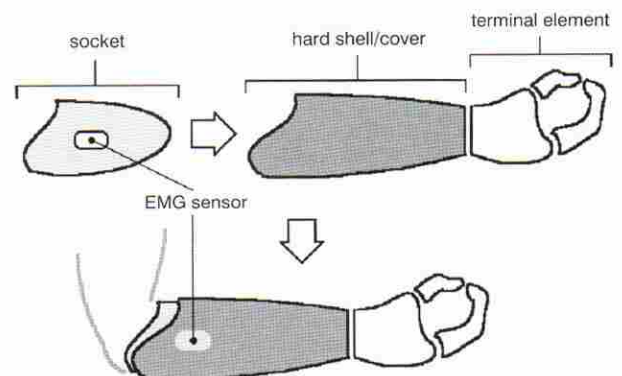
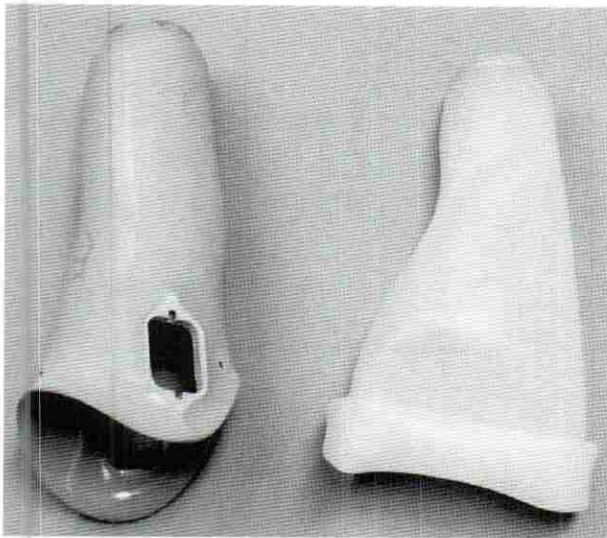


**Fig. 1** Schematic diagram of externally powered below-elbow prosthesis. Currently, EMG sensors are fastened in hard socket wall. Hard shell that holds terminal element is adjusted over hard socket

Correspondence should be addressed to Dr Tom Chau;  
email: tchau@bloorviewmacmillan.on.ca

Paper received 16 August 2002 and in final form 13 January 2003  
MBEC online number: 20033763

© IFMBE: 2003



a

b

**Fig. 2** Comparison of (a) laminated hard socket and (b) soft silicon socket or roll-on sleeve. Rectangular openings in hard socket are intended for EMG sensor attachment. Note that silicon socket has been rolled up to emphasise its flexibility

prosthesis control may allow silicon sleeves to be used in place of hard sockets.

### 1.2 Mechanomyography

Mechanomyography (MMG) is the epidermal measurement of the low-frequency vibrations ('muscular sound') produced by contracting muscles owing to a non-linear summation effect of propagated motor unit twitches and shape changes in muscular fibres during voluntary contraction (ORIZIO *et al.*, 1996). The model of a vibrating string has been consistently used to describe the resonant vibration caused by the effect just described. This model fits well with experimental observations, such as the half-sine like mode of vibration found by OUAMER *et al.* (OUAMER *et al.*, 1999; ZHAO *et al.*, 1994).

The magnitude of the MMG signal is linearly related to muscle strength in non-fatiguing contractions that are between 20 and 80% of the maximum voluntary contraction (MVC) (ORIZIO *et al.*, 1990; ORIZIO, 1993; ZHANG *et al.*, 1992). Most of the power of the MMG signal is located in the 0–45 Hz bandwidth for forearm muscles. No significant components have been found beyond 100 Hz (ORIZIO *et al.*, 1990; ORIZIO, 1993; OUAMER *et al.*, 1999; GOLDENBERG *et al.*, 1991).

### 1.3 MMG and prosthesis control

MMG signals can be measured using microphones (ORIZIO *et al.*, 1990; COURTEVILLE *et al.*, 1998; WATAKABE *et al.*, 2001) or accelerometers (WATAKABE *et al.*, 2001; ZHANG *et al.*, 1992). Some authors suggest microphones for MMG signal recording, as they are less susceptible to motion artifacts. However, higher sensitivity values have been reported for accelerometers (WATAKABE *et al.*, 2001). Through use of multiple accelerometers, it may be possible to eliminate motion artifacts using simple differential recording techniques commonly applied to EMG measurements (CRAM *et al.*, 1998; LOEB and GANS, 1986).

MMG signals recorded by a standard microphone have been used to operate a free-standing prosthetic hand in a controlled, laboratory setting (BARRY *et al.*, 1986). Using a single-channel, full-wave rectified MMG signal and a tristate control strategy, Barry *et al.* demonstrated that two below-elbow amputees could

use intentional MMG to open and close a prosthetic hand. The reported system successfully discriminated between MMG signals arising from wrist flexion and extension and exhibited robustness to changes in skin impedance and microphone placement. However, unresolved sensor attachment and low-frequency noise elimination issues limited its practical usefulness as an alternative prosthesis control signal.

Our objective was to determine whether MMG signals can be recorded using silicon embedded transducers (microphones and accelerometers). This investigation is a step towards the use of soft silicon suction sockets in externally powered prostheses. The experiments discussed here focus only on the characterisation of silicon-embedded accelerometers.

## 2 Materials and methods

To quantify the signal-to-noise ratio (SNR) and frequency responses of silicon-embedded accelerometers, predefined vibration patterns were generated using a custom-made mechanical stimulator. These were applied to standardise excitation to the accelerometers. For comparison, the same measurements were conducted using non-embedded accelerometers as controls.

### 2.1 Preparation of samples

Single-axis micro-machined accelerometers\*, with a mass of 0.28 g and dimensions of  $5.59 \times 2.28 \times 8.56$  mm (width, height and length, respectively), were used for the tests. Fig. 3 shows a schematic diagram of the samples prepared, indicating their embedding parameters, namely, silicon hardness, contact surface, top layer thickness and bottom-layer thickness. Three groups of five accelerometers each were embedded into silicon squares with different hardness values (shores 20A, 35A and 65A) for a total of 15 prepared samples. These were numbered 1–15. Samples 1–5 were embedded using the hardest silicon type (shore 65A), samples 6–10 used the medium silicon type (shore 35A), and samples 11–15 used the softest silicon type (shore 20A). Table 1 shows the numerical values of the top-layer thickness  $T_{TL}$  and bottom-layer thickness  $T_{BL}$  of each sample (see Fig. 3).

### 2.2 Hardware set-up

Fig. 4 shows a block diagram of the system used for the experiments. A 16-bit PC soundcard† was used simultaneously to generate the stimulation pattern and record the sensor response. Stimulus and response signals were amplified, respectively, by gains of  $G_1 = 20$  and  $G_2 = 400$  using LM 386 audio

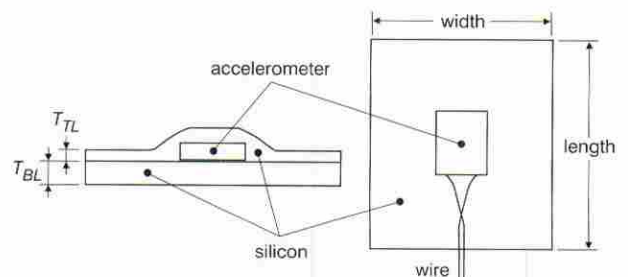


**Fig. 3** Schematic diagram of silicon-embedded accelerometer samples.  $T_{TL}$  = top layer thickness;  $T_{BL}$  = bottom layer thickness

\*BU-7135, Emkay Innovative Products

†SB Live!, Creative Labs

Table 1 Top-layer ( $T_{TL}$ ) and bottom-layer ( $T_{BL}$ ) thickness values of samples prepared

Sample	$T_{TL}$ , mm	$T_{BL}$ , mm
1, 6, 11	$3 \pm 0.5$	$1 \pm 0.5$
2, 7, 12	$2 \pm 0.5$	$1 \pm 0.5$
3, 8, 13	$1 \pm 0.5$	$1 \pm 0.5$
4, 9, 14	$2 \pm 0.5$	$2 \pm 0.5$
5, 10, 15	$2 \pm 0.5$	$3 \pm 0.5$

amplifiers. The mechanical stimulator<sup>‡</sup>, shown in Fig. 5, was a card-type speaker, mounted in a wooden resonance box to ensure good, low-frequency signal reproduction. As we were concerned with relative responses, i.e. the response of the embedded accelerometers relative to the non-embedded accelerometers, the typical requirement for a stimulator with a flat frequency response over the frequencies of interest was not necessary. The speaker has the advantage of being a non-uniform vibrating surface in which the maximum amplitude is at the centre of the speaker. This non-uniform response corresponds to previous reports of real MMG measurements, in which the muscle was described as a vibrating string with a half-sine-like mode of vibration (OUAMER *et al.*, 1999).

### 2.3 Generation of vibration patterns

Two different patterns were electronically generated for SNR determination using the MATLAB environment\*\*. The 'signal' was a summation of scaled in-phase sinusoidal signals from 1 to 100 Hz (ten frequencies per decade, in equally spaced intervals). Once amplified and sent to the stimulator, the magnitude of the peak frequency (20 Hz) resembled that of real MMG signals at approximately 75% of MVC ( $0.3 \text{ ms}^{-2}$ ). This estimate was obtained by linearly extrapolating from previously reported measurements, where an MMG signal amplitude of approximately  $0.08 \text{ ms}^{-2}$  corresponded to 20% of MVC (WATAKABE *et al.*, 2001). The 'noise' consisted of band-limited white noise, the maximum magnitude of which was 15% of the peak 'signal' magnitude.

### 2.4 Test methodology

We tested different embedding properties to determine if there were significant trends in sensor performance. For SNR quantification, two different stimuli were separately applied to each sample, one being a pure noise signal and the other a signal with added noise. The measurement of the signal with added noise presented a more accurate way to obtain the SNR value (rather than measuring the signal by itself), as it was impossible completely to eliminate the background noise during measurements. SNR values were calculated as follows:

$$SNR = 10 \log \left[ \left( \frac{RMS_{SIGNAL+NOISE}}{RMS_{NOISE}} - 1 \right)^2 \right] \quad (1)$$

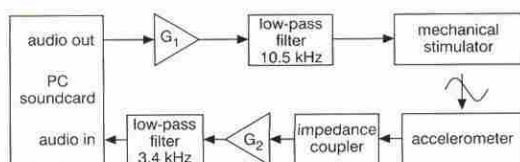


Fig. 4 Block diagram of instrumented system for stimulating and recording response from sensors

<sup>‡</sup>WM-R57A, Panasonic

\*\*MathWorks Inc

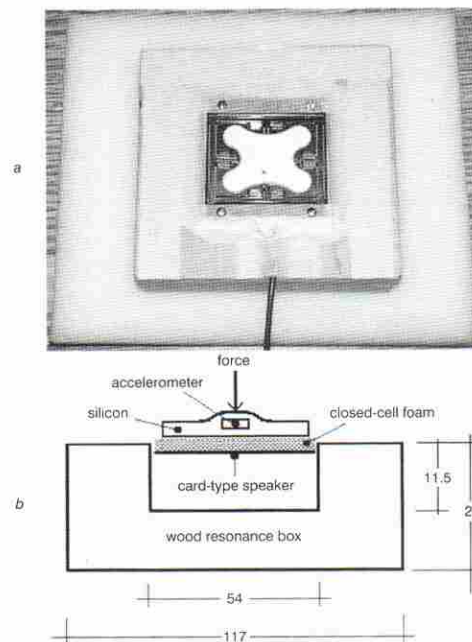


Fig. 5 (a) Top view and (b) schematic diagram of mechanical stimulator built for measurements. Placement of embedded samples is shown in schematic diagram. All dimensions are in millimetres

The subtraction of 1 is a correction factor that allowed us to obtain the actual value of SNR for the worst case in which the noise is completely additive (or in phase with the signal).

Fig. 5 shows the vector representing the static forces that were carefully applied directly over each sample, emulating the force of the skin against the sensor within an externally powered prosthesis. Owing to the nature of the applied force and the geometrical differences among samples, the exact amount of force could not be precisely determined. However, it was possible to ensure that all forces were in the 0.2–0.5 N range.

Fig. 6 shows the actual mechanical coupling of the samples to the vibrating surface. A weight was placed over the supporting ring. This applied an evenly distributed force on the foam along the ring's perimeter. In turn, this force compressed the foam, generating a distributed position-dependent force over the sample. A similar effect would be present within a silicon sleeve in externally powered prostheses. Four values of increasing force ( $F_1$ – $F_4$ ) were produced by gradually incrementing the weight on top of the supporting ring by a constant amount. These forces were deemed to be comparable with the real forces experienced by sensors within a soft silicon socket, pressing against the skin.

Three sets of recordings (including force variations) were acquired using different contact surface values, to evaluate their effects on the SNR. The three surfaces tested were  $32 \times 42 \text{ mm}^2$ ,  $22 \times 32 \text{ mm}^2$  and  $12 \times 22 \text{ mm}^2$  (width and length, respectively). The independent variables tested were thus silicon hardness, the thickness of both the top and bottom layers of embedding, the contact surface and the applied force. For frequency response determination, the samples were systematically excited with scaled sinusoidal signals ranging from 1 to 4000 Hz (ten frequencies per decade in equally spaced intervals), with magnitudes close to  $0.3 \text{ ms}^{-2}$ . The lower limit of this range (1 Hz) is defined by the lowest frequency signal that can be reproduced by the stimulating system. The upper limit is defined by the maximum frequency that can be reliably measured (approximately 11 points per cycle), given the maximum sampling frequency of the soundcard. Root mean square (RMS) and phase values of signals obtained from the sensors were automatically calculated and stored for further analysis.

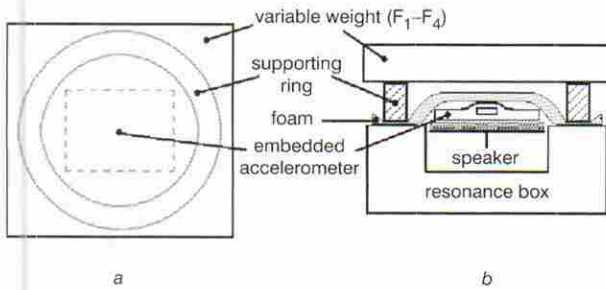


**Fig. 6** Mechanical coupling of tested samples to vibrating surface of stimulator. (a) Top view. (b) Front view

### 2.5 Test validation

Ten repeated measurements for each of the 15 samples with each contact surface and each force applied were recorded. The Lilliefors test for normality (CONOVER, 1999) was applied to the set of SNR calculations of each sample. As some data did not follow a normal distribution, we used the Wilcoxon–Mann–Whitney rank sum one-sided test to determine whether or not the SNR values obtained for a certain combination of variables were significantly higher than those of the non-embedded sensors.

To test the hypothesis of independence between the SNR and the other variables, the data were first organised into sensor groups. A sensor group is defined as a collection of samples that differ in only one variable (silicon type, top layer thickness, bottom layer thickness, surface area or applied force). Subsequently, we constructed a contingency table with the observed frequencies of increasing, decreasing or non-monotonic trends in SNR. A Monte-Carlo simulation with  $10^6$  groups of random numbers provided the expected frequencies under the null hypothesis of no monotonic relationships between SNR and the independent variables. A  $\chi^2$  test for goodness-of-fit was used to test this null hypothesis. Finally, an adjusted residuals matrix (CHRISTENSEN, 1990) was computed to determine which types of trend were significantly different from the expected values. For all statistical tests, a 5% significance level ( $\alpha = 0.05$ ) was used.

For the frequency behaviour determination, ten repeated measurements were taken for each frequency tested. The relative response in both magnitude and phase was calculated. The reference in this case (0 dB and 0 degrees, respectively) was always the non-embedded accelerometer response. This method ensured that differences observed were due strictly to the embedding and not to the combined effects of the amplifier, the speaker or the soundcard itself.

## 3 Results

Table 2 shows the mean values and standard deviations of SNR obtained for embedded and non-embedded accelerometers for each force applied. Forces are labelled as  $F_1$ – $F_4$  identifying increasing forces (increasing weights on top of the supporting ring, shown in Fig. 6). Note that the mean SNR values of embedded accelerometers were significantly higher than those of their non-embedded counterparts ( $p < 0.01$  for each group

from  $F_1$  to  $F_4$ , and  $p = 0.0028$  for the whole set). With the exception of a few samples (mainly the medium silicon hardness samples), this behaviour was consistently repeated also within sensor groups.

From the Monte-Carlo simulation, we obtained values of 0.16, 0.16 and 0.66 for the probabilities of increasing, decreasing and non-monotonic trends, respectively. From the  $\chi^2$  test, we determined that the SNR is dependent on all of the variables tested. Finally, from residual analysis, the significant trends in the above dependencies were as follows. The SNR increased as

- (i) the bottom layer thickness increased
- (ii) the top layer thickness increased
- (iii) the contact surface area decreased
- (iv) the hardness of the silicon decreased

No significant trend was found for variations in applied force.

Fig. 7 shows the typical SNR values obtained for the most representative sensor groups for each variable tested. These graphs clearly reflect the trends described above. Note the relatively high  $R^2$  values for each regression. Fig. 8 shows a bode plot of one of the samples tested (hardest silicon, medium contact surface, lowest applied force). Note that there were no considerable phase shifts within the 5–100 Hz bandwidth. None of the samples showed a considerable deviation from this behaviour.

Fig. 9 shows the general form of the relative magnitude response for silicon embedded accelerometers. Compared with their non-embedded counterparts, the embedded accelerometers behaved as a band-stop filter whose rejection band C fell an average of 20 dB in the 300–900 Hz bandwidth, with a ripple  $R_1$  from about 10 to 20 dB wide. The low-pass band A extended from 5 to 100 Hz. This is the bandwidth of interest for the proposed application. Note that, here, the response is relatively flat.

There were no significant changes in the frequency response due to changes in the applied force. However, the silicon hardness and contact surface of embedding did considerably affect the relative magnitude response of the sample in this region. A peak occurred in region B at 200 Hz. The high-pass band D began at 1000 Hz and presented a ripple  $R_2$  of up to 20 dB wide. In most cases, within this band D, a peak occurred at 1000 or 2000 Hz, rising about 5 dB above the low-pass band level A.

The broken lines in the low-pass band represent the maximum deviation from the general form of the response. Deviation in section A was attributed to the medium silicon hardness (shore 35A). Deviation in section B was elicited by changes in the contact surface such that, as the contact surface increased, the peak at 200 Hz tended to disappear.

As an aside, Fig. 10 depicts a real MMG signal recorded from the wrist flexors using a silicon-embedded accelerometer. This verifies that silicon-embedded accelerometers can indeed be used to record real MMG signals.

## 4 Discussion

It is possible that some of the variations in the measured responses were influenced by the mechanical characteristics of

*Table 2* SNR values (dB) measured in embedded and non-embedded transducers. Increasing applied forces are labelled  $F_1$ – $F_4$

Samples	Force			
	$F_1$	$F_2$	$F_3$	$F_4$
Non-embedded	12.42 ± 0.03	10.54 ± 0.13	11.73 ± 0.02	9.21 ± 0.03
Embedded	19.86 ± 3.91	19.18 ± 3.98	19.07 ± 3.74	18.70 ± 4.31

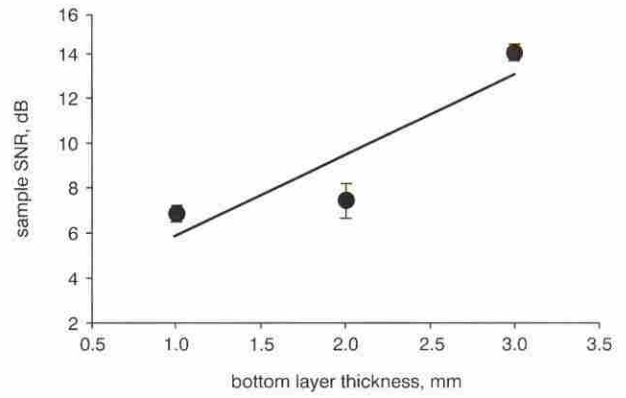
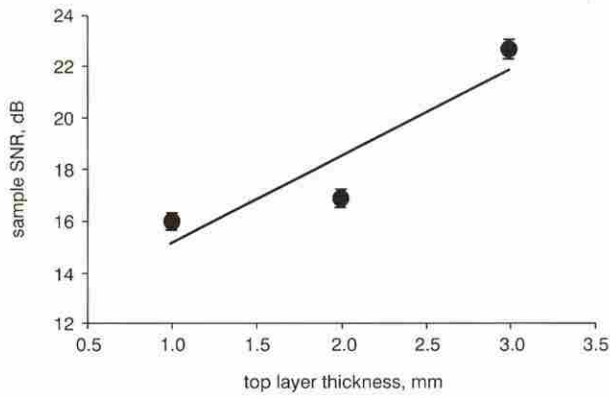
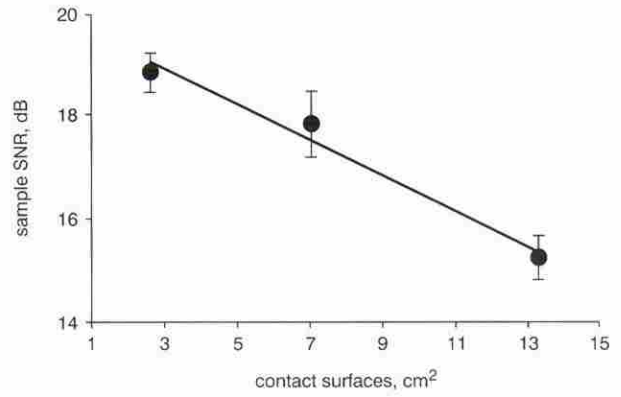
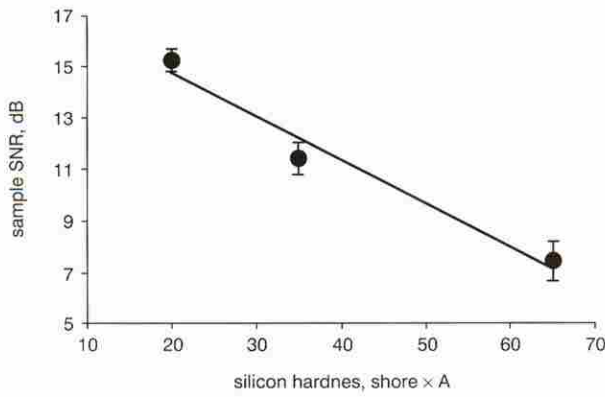


**Fig. 7** Typical results obtained from most representative sensor groups for each variable tested. (a) Silicon hardness test;  $R^2 = 0.909$ . (b) Contact surface test;  $R^2 = 0.978$ . (c) Top layer thickness test;  $R^2 = 0.849$ . (d) Bottom layer thickness test;  $R^2 = 0.808$ . Each graph shows linear regression

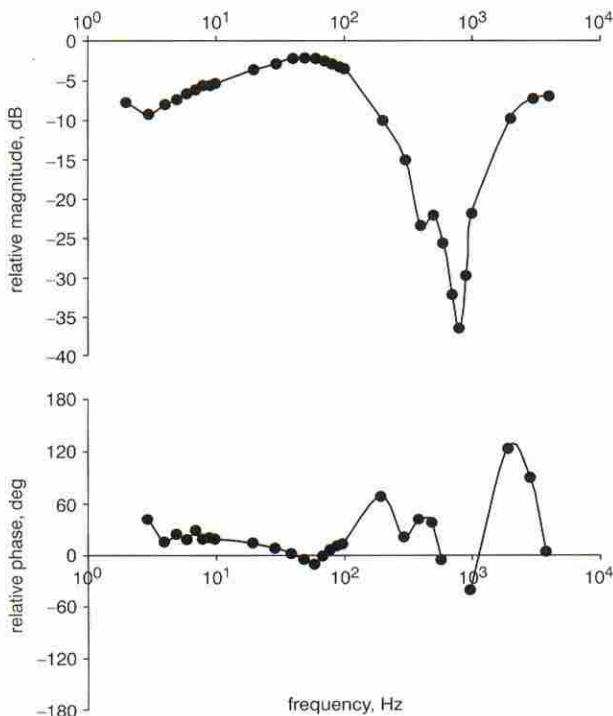


**Fig. 8** Sample bode plot of one of samples tested. Reference for each frequency (0dB, 0 degrees) is non-embedded transducer response

the system. This is especially true for the contact surface tests and, possibly, for the thickness tests (of both top and bottom layers). Changes in the mass of the complete system were inherent to both tests. Increments in mass added static forces to the system. In some samples, especially the ones with the highest mass values, these forces were comparable with the externally applied forces tested. Hence, rather than gauging relationships between the SNR and various independent variables, a more precise observation might be that the SNR of embedded samples increased with increasing, but concentrated,

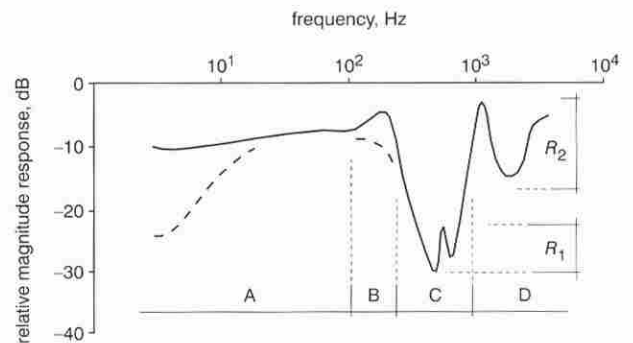


**Fig. 9** General form of embedded accelerometers' relative magnitude. A: Low-pass band. B: Peak frequency band. C: Reject band. D: High-pass band.  $R_1$  = reject band ripple.  $R_2$  = high-pass band ripple. (---) Maximum deviation from general form in region A was due to silicon hardness and contact surface variations

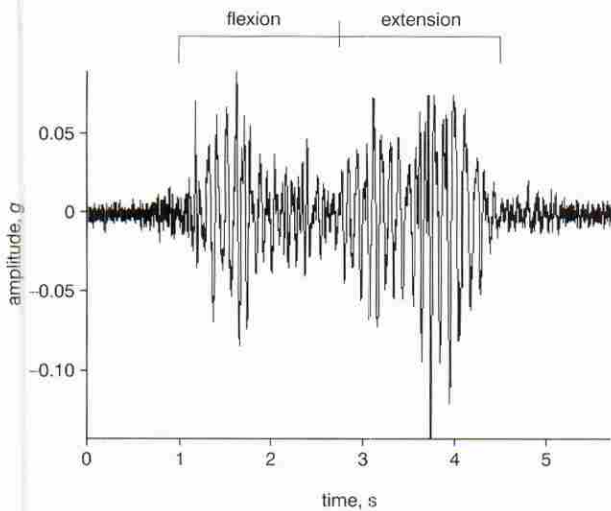


**Fig. 10** Example of actual MMG signal recorded using silicon-embedded accelerometer. Vertical axis is in units of gravitational acceleration  $g$

mass and applied force. This statement is consistent with the nature of the mechanical stimulator. As the stimulator was based on a vibrating membrane mechanically grounded along its perimeter, the magnitude of the vibrations would be higher towards the centre of the speaker. As mentioned earlier, this behaviour simulates previously reported longitudinal amplitude losses in real MMG measurements. Nonetheless, in the future, it is necessary to confirm the observed sensor performance in real MMG measurements.

Recall that MMG signals have no significant frequency components beyond 100 Hz. Therefore frequency components occurring in the C and D bands in Fig. 9 can be considered noise. The mechanical properties of silicon naturally provide considerable noise damping within the C band. Further noise suppression within the C and D bands can be achieved using either hardware or software filtering.

## 5 Conclusions

From the results we can state that

- The SNR of embedded accelerometers is consistently higher than that of their non-embedded counterparts making the former suitable for MMG signal recording.
- The reject band in the frequency response of embedded samples is wide enough to eliminate higher-frequency noises.
- The softest or the hardest silicon types (shores 20A and 65A) are recommended for MMG measurements, as they exhibited the least variability during the tests.
- Although there seem to be clear relationships between sensor performance and the variables tested, experimentation with real MMG recording is required further to validate these findings.

The reported findings do show however, that it is feasible to embed accelerometers in a soft silicon suction socket for MMG signal acquisition for externally powered prosthesis control.

**Acknowledgments**—The authors would like to acknowledge the support of the Bloorview MacMillan Children's Foundation, the Natural Sciences Engineering Research Council of Canada, the Hospital for Sick Children Foundation and the Bloorview Children's Hospital Foundation.

## References

- BARRY, D. T., LEONARD, J. A., GLITTER, A. J., and BALL, R. D. (1986): 'Acoustic myography as a control signal for an externally powered prosthesis', *Arch. Phys. Med. Rehabil.*, **67**, pp. 267–269
- CHRISTENSEN, R. (1990): 'Log-linear models' (Springer-Verlag, 1990), pp. 154–161
- CONOVER, W. J. (1999): 'Practical non-parametric statistics' (John Wiley & Sons, 1999), pp. 443–447
- COURTEVILLE, A., GHARBI, T., and CORNU, J. Y. (1998): 'MMG measurement: a high-sensitivity microphone-based sensor for clinical use', *IEEE Trans. Biomed. Eng.*, **45**, pp. 145–150
- CRAM, J., KASMAN, G., and HOLTZ, J. (1998): 'Introduction to surface electromyography' (Aspen Publishers Inc., 1998), pp. 49–50
- GABER, T. A. Z. K., GARDNER, C. M., and KIRKER, S. G. B. (2001): 'Silicone roll-on suspension for upper limb prosthesis: user's views', *Prosthet. Orthot. Int.*, **25**, pp. 113–118
- GOLDENBERG, M. S., YACK, H. J., CERNY, F. J., and BURTON, H. W. (1991): 'Acoustic myography as an indicator of force during sustained contractions of a small hand muscle', *J. Appl. Physiol.*, **70**, pp. 87–91
- LOEB, G., and GANS, C. (1986): 'Electromyography for experimentalists' (The University of Chicago Press, 1986), pp. 18–19
- ORIZIO, C., PERINI, R., DIEMONT, B., MARANZANA FIGINI, M., and VEICSTEINAS, A. (1990): 'Spectral analysis of muscular sound during isometric contraction of biceps brachii', *J. Appl. Physiol.*, **68**, pp. 508–512
- ORIZIO, C. (1993): 'Muscle sound: bases for the introduction of a mechanomyographic signal in muscle studies', *Crit. Rev. Biomed. Eng.*, **21**, pp. 201–243
- ORIZIO, C., LIBERATI, D., LOCATELLI, C., DE GRANDIS, D., and VEICSTEINAS, A. (1996): 'Surface mechanomyogram reflects muscle fibres twitches summation', *J. Biomech.*, **29**, pp. 475–481
- OUAMER, M., BOITEUX, M., PETITEJEAN, M., TRAVENS, L., and SALÈS, A. (1999): 'Acoustic myography during voluntary isometric contraction reveals non-propagative lateral vibration', *J. Biomech.*, **32**, pp. 1279–1285
- WATAKABE, M., MITA, K., AKATAKI, K., and ITOH, Y. (2001): 'Mechanical behaviour of condenser microphone in mechanomyography', *Med. Biol. Eng. Comput.*, **39**, pp. 195–201
- ZHANG, Y. T., BASIL, C., MANDAYAM, R., and DOUGLAS, G. (1992): 'A comparative study of simultaneous vibromyography and electromyography with active human quadriceps', *IEEE Trans. Biomed. Eng.*, **39**, pp. 1045–1052
- ZHAO, L. Q., ZHANG, Y. T., HERZOG, W., and YUAN, D. F. (1994): 'A theoretical study of muscle vibrations: the influence of transducer mass on vibromyographic signals.' *Proc. CMBES Conf., CMBEC 20*, pp. 16–17

## Authors' biographies

JORGE SILVA is a graduate student in the Mechanical and Industrial Engineering Department and the Institute of Biomaterials and Biomedical Engineering at the University of Toronto. His current research interests lie in robotics, digital signal processing, intelligent and adaptive systems and pattern recognition.

TOM CHAU is a research coordinator at Bloorview MacMillan Children's Centre and Assistant Professor at the Institute of Biomaterials and Biomedical Engineering, University of Toronto. His research focuses on the development and evaluation of intelligent systems and devices for paediatric rehabilitation.

STEVE NAUMANN is Director of Rehabilitation Engineering at Bloorview MacMillan Children's Centre, Prosthetics and Orthotics Team Leader of the Ontario Rehabilitation Technology Consortium, and Associate Professor, Institute of Biomaterials and Biomedical Engineering. His research interests are gait analysis and movement control in neuromusculoskeletal disorders, orthotics, lower-limb and electrically powered upper-limb prosthetics, and general development and assessment of assistive devices.

WINFRIED HEIM is a certified prosthetist at Bloorview MacMillan Children's Centre and is pursuing graduate studies in the Prosthetics and Orthotics Department, University of Strathclyde, Scotland. His research interests are upper and lower limb prostheses, the fit, suspension and control of prostheses and related outcome measures.

